AIAA JOURNAL
Vol. 41, No. 2, February 2003

Low-Reynolds-Number k–$\tilde{\epsilon}$ Modeling of Nonstationary Solid Boundary Flows

C. B. Hwang* and C. A. Lin†
National Tsing Hua University, Hsinchu 300, Taiwan, Republic of China

An improved low-Reynolds-number k–$\tilde{\epsilon}$ model is adopted to predict turbulent flows with a nonstationary boundary. The performance of the adopted model is first contrasted with direct numerical simulation data of the turbulent plane Couette–Poiseuille flow. Detailed flow structure is captured accurately by the model, in particular the reduction of the shear stress and, hence, the turbulent kinetic energy due to the presence of the moving wall. The validity of the present model in computing complex flows within rotating disk cavities is further examined. Flows with two different rotational Reynolds numbers are investigated, and the predicted mean and turbulence results are also contrasted with measurements. The influence of rotation on the flowfield and turbulence modeling is investigated by sensitizing the turbulence model coefficient to rotational Richardson number, and the effect is found to be marginal. Because the internal flow structure of the rotating disk cavities is induced by the diffusive transport of the tangential momentum from the rotor into the interior, the predicted thickness of the Ekman layer is found to be critical to the correct predictions. The adopted model reproduces correctly the gradual thickening of the Ekman layers from small to large radii, which is due to the transition from laminar to turbulent regimes, especially on the rotor side within the disk cavities. The elevated level of turbulence on the stator side compared to that on the rotor side is also predicted correctly by the present model.

Introduction

FLOWS with a nonstationary boundary attract considerate attention from engineers due to their frequent industrial applications. Depending on the specific device investigated, the influences of the moving wall on the device flow structure may differ. The moving wall of the turbulent plane Couette–Poiseuille flow, for example, can cause the asymmetric axial velocity distribution across the channel. Hence, because of the reduction of the shear stress at the moving wall, the turbulent kinetic energy adjacent to the moving boundary is severely damped.

Another typical example is the enclosed rotor–stator case, where no external through flow is present across the disk boundary. Despite the simplicity of the geometry, its flowfield is rather complex. The internal flowfield is induced by the diffusive transport of tangential momentum from the rotor wall into the cavity interior. Therefore, the thin boundary layer (the Ekman layer), on the wall exerts significant influence on the momentum transport and also heat transfer, and, hence, intense interaction of wall and the internal flowfields exist. Two distinct features characterize the flowfield. The first one is the single circulating vortex caused by the imbalance of centrifugal forces that produce the radial outflow over the rotor side and a radial inflow over the stator side, and the second is the gradual transition from laminar to turbulent flow when the flow travels to large radii. An inviscid core exists between the two thin boundary layers so that the radial velocity is virtually zero. Comprehensive discussions of the rotating disk cavity flows can be found in Refs. 1 and 2.

Despite its geometric simplicity, numerical predictions of the enclosed rotor–stator flowfields, for example, are restrained by various obstacles, such as the numerical accuracy and the representation of turbulence.[3–7] With the advances of computer capacity, relatively fine grids can be achieved in the two-dimensional simulations incorporating higher order of discretization schemes. The remaining obstacle is, however, the modeling of turbulence. The effects of the moving wall or rotation on the turbulence field and the possible coexistence of laminar and turbulent regions make it a difficult task. However, few of the previous proposed models are capable of reproducing the complex flow characteristics in the rotor–stator system.[7] One major discrepancy is due to the failure of the models to predict transition. The other drawback is the inadequate modeling of the turbulence transport processes in the vicinity of the wall.

Earlier numerical investigations[3] have shown that the wall function approximation does not deliver accurate resolution of the thin Ekman layer region. Over the years, many substitutions for the wall function approach had been made. However, the forms of these models were based on ad hoc adjustments of the model constants and damping functions to reproduce the flowfield. To remedy these drawbacks, an improved form of low Reynolds number two-equation turbulence model was proposed.[8] However, the model was not tested in the rotor–stator environment.[9,10]

It is generally accepted that the Coriolis force can considerably affect turbulent flows. Traditionally, these effects are investigated by studying parallel shear flows under orthogonal mode rotation, that is, when the axis of rotation is either parallel or antiparallel to the mean flow vorticity vector. Turbulence is usually suppressed if the rotation vector is parallel to the vorticity vector and enhanced if they are antiparallel. This is similar to the stabilizing and destabilizing effects for a shear flow entering a convex and a concave curvature. Thus it was suggested that the Reynolds stress transport model is needed to deal with the complex flows present in rotating cavity flows.[11–13]

Computations of Elena and Schiestel[12] indicated that, although the Reynolds stress transport model (RSTM) (see Hanjalic and Launder[14]) performs better at the stator side, its performance at the rotor side is surprisingly similar to the k–ϵ model (Launder and Sharma[15]). Both models show reduced levels of diffusion at the rotor side. Therefore, the capability of the inherent interaction of swirl and turbulence present in the RSTM model does not seem to play a major role. There may be another mechanism, which is absent in the models. Elena and Schiestel[13] further improved their results by adding rotation and local vorticity sensitized empirical terms in the k equation. The effect of this term is to increase the turbulence level at the rotor side. It was argued that these are to model the effect of the pressure diffusion process at this region, which is absent in the model of Hanjalic and Launder.[14] Therefore, this seems to suggest that accurate near-wall modeling is important in the present rotor–stator geometry.

Received 14 August 2001; revision received 6 February 2002; accepted for publication 16 September 2002.

*Graduate Student, Department of Power Mechanical Engineering.
†Professor, Department of Power Mechanical Engineering. Senior Member AIAA.

However, the approaches adopted by Elena and Schiestel[13] are empirical and ad hoc treatments. On the other hand, the Reynolds transport transport models are expensive computationally. This has motivated the present study to examine how the proposed model[8] behaves in this complex environment.

The predictive performance of the model is assessed by comparisons with direct numerical simulation (DNS) data and measurements. The plane Couette–Poiseuille flows and the enclosed rotating cavity flows form the basis of investigations. The plane Couette–Poiseuille flows are designed to examine the model's performance to predict the reduction of the shear stress, hence, turbulence level, at the moving wall. The enclosed rotating disk flows are adopted to explore the turbulence model's capability to simulate the complex flows within the disk cavities. The effect of rotation on the flow structure is also explored using the rotational Richardson number approach (see Refs. 2 and 16). The present study will help to examine the influences of the refined wall modeling on these flows within the eddy-viscosity framework.

Turbulence Modeling

Although the present applications are concerned with flows with a nonstationary boundary, the equations are expressed using the inertia frame of reference. Within the framework of eddy viscosity and adopting the Boussinesq approximation, the time-averaged momentum equation for high Reynolds number flow may be described as follows (in terms of Cartesian tensor):

$$\frac{\partial(\rho U_i U_j)}{\partial x_j} = -\frac{\partial P}{\partial x_i} + \frac{\partial}{\partial x_j}\left[\rho(\nu + \nu_t)\left(\frac{\partial U_i}{\partial x_j} + \frac{\partial U_j}{\partial x_i}\right)\right] \tag{1}$$

where ν_t is the turbulent kinematic eddy viscosity.

In the present applications, the turbulence model adopted is the k–$\tilde{\varepsilon}$ model.[15] When the model is applied toward the wall, the contribution of molecular viscosity on the shear stress increases, and the standard high-Reynolds-number turbulence model must be modified to account for the diminishing effect of the near-wall turbulence levels. The construction of the low-Reynolds-number model is the focus of the next section.

Near-Wall Modeling

The exact form of the transport equation for turbulent kinetic energy can be expressed as[17]

$$\frac{\partial U_j k}{\partial x_j} = \underbrace{\frac{\partial}{\partial x_j}\left(\nu\frac{\partial k}{\partial x_j}\right)}_{\mathcal{D}_k} \underbrace{-\frac{\partial}{\partial x_j}\left(\frac{1}{2}\overline{u_i u_i u_j}\right)}_{\mathcal{T}_k} \underbrace{-\frac{1}{\rho}\frac{\partial}{\partial x_j}(\overline{pu_j})}_{\Pi_k}$$
$$\underbrace{-\overline{u_i u_j}\frac{\partial U_i}{\partial x_j}}_{\mathcal{P}_k} \underbrace{-\nu\overline{\frac{\partial u_i}{\partial x_j}\frac{\partial u_i}{\partial x_j}}}_{\varepsilon} \tag{2}$$

where $\mathcal{D}_k$, $\mathcal{T}_k$, Π_k, $\mathcal{P}_k$, and ε are the laminar diffusion, turbulent diffusion, pressure diffusion, turbulent production, and turbulent dissipation rate, respectively.

The commonly adopted approach to model the turbulent diffusion term and the pressure diffusion term is to adopt a general gradient diffusion hypothesis, that is,

$$\frac{\partial}{\partial x_j}\left[\frac{\nu_t}{\sigma_k}\frac{\partial k}{\partial x_j}\right] = \underbrace{-\frac{\partial}{\partial x_j}\left(\frac{1}{2}\overline{u_i u_i u_j}\right)}_{\mathcal{T}_k} \underbrace{-\frac{1}{\rho}\frac{\partial}{\partial x_j}(\overline{pu_j})}_{\Pi_k} \tag{3}$$

where σ_k is the Prandtl number for k.

However, this modeling practice is only appropriate in the high-Reynolds-number regime, whereas in the near-wall region, the asymptotic behaviors of the turbulent diffusion term and the pressure diffusion term are different.

This can be verified by examining first the variations of the instantaneous velocity components with the distance from the wall y. Following Launder,[17] this can be expressed as

$$u = b_1 y + c_1 y^2 + d_1 y^3 + \cdots \tag{4}$$

$$v = c_2 y^2 + d_2 y^3 + \cdots \tag{5}$$

$$w = b_3 y + c_3 y^2 + d_3 y^3 + \cdots \tag{6}$$

where the coefficients b_i, c_i, and d_i are functions of time whose mean value must be zero because $\overline{u_i} = 0$.

When the y-dependent turbulent quantities are inserted into the k equation, it can be shown that, in the near-wall region, the following prevails:

$$\frac{\partial}{\partial x_j}\left[\frac{\nu_t}{\sigma_k}\frac{\partial k}{\partial x_j}\right] \approx \mathcal{O}(y^3) \tag{7}$$

$$\underbrace{-\frac{\partial}{\partial x_j}\left(\frac{1}{2}\overline{u_i u_i u_j}\right)}_{\mathcal{T}_k} \approx \mathcal{O}(y^3) \tag{8}$$

$$\underbrace{-\frac{1}{\rho}\frac{\partial}{\partial x_j}(\overline{pu_j})}_{\Pi_k} \approx \mathcal{O}(y) \tag{9}$$

If the modeling of the pressure diffusion term takes the form of Eq. (3), the contribution of the pressure diffusion process will be absent in the near-wall region. This has profound effect on the predicted near-wall turbulent dissipation rate level. Most models show that the dissipation rate reaches its maximum value somewhere inside the viscous sublayer. However, DNS data indicate that the maximum value of dissipation rate should be located at the wall itself. These, as argued by Kawamura,[18] necessitate the inclusion of Π_k in the k equation, especially in the near-wall region. DNS data indicate that the influences of the pressure diffusion term decay rapidly away from the wall; therefore, Π_k is modeled as[18]

$$\Pi_k = -\frac{1}{2}\nu\frac{\partial}{\partial x_j}\left[\frac{k}{\varepsilon}\frac{\partial\hat{\varepsilon}}{\partial x_j}\right] \approx \mathcal{O}(y) \tag{10}$$

where $\hat{\varepsilon}$ is defined as $\hat{\varepsilon} = 2\nu(\partial\sqrt{k}/\partial x_l)(\partial\sqrt{k}/\partial x_l)$.

It is also apparent that $\hat{\varepsilon}_w$ stands for the nonzero value of dissipation rate at the wall ε_w. Because $\hat{\varepsilon}$ approaches 0 at about $y^+ > 15$, this formulation makes the influence of Π_k confined to the wall region.

Similar approach can be applied to model the equation of the turbulent dissipation rate. The commonly adopted form of the $\tilde{\varepsilon}$ equation can be expressed as[15]

$$\frac{\partial U_j\tilde{\varepsilon}}{\partial x_j} = \frac{\partial}{\partial x_j}\left(\nu\frac{\partial\tilde{\varepsilon}}{\partial x_j}\right) + \frac{\partial}{\partial x_j}\left(\frac{\nu_t}{\sigma_\varepsilon}\frac{\partial\tilde{\varepsilon}}{\partial x_j}\right)$$
$$+ C_{\varepsilon 1} f_1 \mathcal{P}_k\frac{\tilde{\varepsilon}}{k} - C_{\varepsilon 2} f_2\frac{\tilde{\varepsilon}^2}{k} + \cdots \tag{11}$$

where $\tilde{\varepsilon}$ is defined as the difference of ε and $\hat{\varepsilon}$. The asymptotic behavior of $\tilde{\varepsilon}$ is

$$\tilde{\varepsilon} = \varepsilon - \hat{\varepsilon} \approx \mathcal{O}(y^2) \tag{12}$$

The advantage of this approach is that $\tilde{\varepsilon}$ reaches zero at the wall and that $\tilde{\varepsilon}$ equals to ε at about $y^+ > 15$, where $\hat{\varepsilon}$ approaches 0.

In the vicinity of the wall, convection, turbulent diffusion, and production go to zero very rapidly, and the asymptotic behavior of the remaining term is

$$\frac{\partial}{\partial x_j}\left[\nu\frac{\partial\tilde{\varepsilon}}{\partial x_j}\right] \approx \mathcal{O}(1) \tag{13}$$

This necessitates the inclusion of the pressure diffusion to balance the equation, and the form adopted is[8,17]

$$\Pi_{\tilde{\varepsilon}} = -\nu \frac{\partial}{\partial x_j}\left[\frac{\tilde{\varepsilon}}{k}\frac{\partial k}{\partial x_j}\right] \approx \mathcal{O}(1) \tag{14}$$

The idea of the inclusion of $\Pi_{\tilde{\varepsilon}}$ to balance the molecular diffusion at the wall was also adopted by Kawamura,[18] although with a different formulation. However, only the present formulation mimics the diffusive nature of the pressure diffusion term. Furthermore, the proposed modeled $\Pi_{\tilde{\varepsilon}}$ also generates the extra source for ε in the buffer zone, completely replacing the commonly adopted function, $\nu\nu_t(\partial^2 U_i/\partial x_j \partial x_k)(\partial^2 U_i/\partial x_j \partial x_k)$.

Based on the preceding approach, an improved low-Reynolds-number k–$\tilde{\varepsilon}$ model[8] was proposed and takes the form

$$\nu_t = 0.09 f_\mu(y_\lambda)\frac{k^2}{\tilde{\varepsilon}} \tag{15}$$

$$\frac{\partial U_j k}{\partial x_j} = \frac{\partial}{\partial x_j}\left[\nu\frac{\partial k}{\partial x_j}\right] + \frac{\partial}{\partial x_j}\left[\frac{\nu_t}{\sigma_k}\frac{\partial k}{\partial x_j}\right] \underbrace{-\frac{1}{2}\nu\frac{\partial}{\partial x_j}\left[\frac{k}{\varepsilon}\frac{\partial \hat{\varepsilon}}{\partial x_j}\right]}_{\Pi_k}$$

$$-\overline{u_i u_j}\frac{\partial U_i}{\partial x_j} - (\tilde{\varepsilon} + \hat{\varepsilon}) \tag{16}$$

$$\frac{\partial U_j \tilde{\varepsilon}}{\partial x_j} = \frac{\partial}{\partial x_j}\left[\nu\frac{\partial \tilde{\varepsilon}}{\partial x_j}\right] + \frac{\partial}{\partial x_j}\left[\frac{\nu_t}{\sigma_{\tilde{\varepsilon}}}\frac{\partial \tilde{\varepsilon}}{\partial x_j}\right] \underbrace{-\nu\frac{\partial}{\partial x_j}\left[\frac{\tilde{\varepsilon}}{k}\frac{\partial k}{\partial x_j}\right]}_{\Pi_{\tilde{\varepsilon}}}$$

$$-C_{\epsilon 1}\overline{u_i u_j}\frac{\partial U_i}{\partial x_j}\frac{\tilde{\varepsilon}}{k} - C_{\epsilon 2}\frac{\tilde{\varepsilon}^2}{k} \tag{17}$$

where $y_\lambda = y/\sqrt{(\nu k/\tilde{\varepsilon})}$. Here $\sqrt{(\nu k/\tilde{\varepsilon})}$ is the Taylor microscale, and Π_k and $\Pi_{\tilde{\varepsilon}}$ are pressure diffusion terms in the k and $\tilde{\varepsilon}$ equations. The coefficients of the model are set to be $C_{\epsilon 1} = 1.44$, $C_{\epsilon 2} = 1.92$, $f_\mu = 1 - \exp(-0.01 y_\lambda - 0.008 y_\lambda^3)$, $\sigma_k = 1.4 - 1.1\exp(-y_\lambda/10)$, and $\sigma_{\tilde{\varepsilon}} = 1.3 - 1.0\exp(-y_\lambda/10)$.

The adoption of y_λ avoids the obvious defect, that is, the singularity occurring at the reattaching point by adopting $y^+ = U_\tau y/\nu$. The damping functions are chosen to retain the high-Reynolds-number form away from the solid boundaries. The asymptotic values of the turbulent Prandtl numbers σ_k and $\sigma_{\tilde{\varepsilon}}$ are adopted as 0.3 to obtain sufficient dissipation rate in the vicinity of the wall. In the core region of the flow, $\sigma_k > \sigma_{\tilde{\varepsilon}}$ is chosen to eliminate the common drawback that turbulent diffusion of k overwhelms that of ε (Ref. 19).

The adopted form of f_μ reproduces correctly the asymptotic limit, that is, $f_\mu \propto y$, and, hence, $-\overline{uv} \propto y^3$ toward the wall. The satisfaction of the asymptotic limit also guarantees the correct level of ε with the maximum locating at the wall itself. This modification is important to mimic properly the turbulence levels and transfer rates as a wall is approached.

Here, the performance of the commonly used k–$\tilde{\varepsilon}$ model proposed by Launder and Sharma (LS),[15] which was rated best in the reviews of Patel et al.[20] and Savill,[21] is to be contrasted with the present model's predictions.

Modeling Rotational Effects

In a rotating frame of reference, the momentum equation can be expressed as

$$\frac{\partial(\rho U_i U_j)}{\partial x_j} = -\frac{\partial P}{\partial x_i} + \frac{\partial}{\partial x_j}\left[\rho(\nu + \nu_t)\left(\frac{\partial U_i}{\partial x_j} + \frac{\partial U_j}{\partial x_i}\right)\right] - 2\epsilon_{ijk}\boldsymbol{\Omega}_j U_k \tag{18}$$

where ϵ_{ijk} and $\boldsymbol{\Omega}_j$ are cyclic permutation tensor and rotating frame vector, respectively.

To model the rotational effect on turbulence structure within the eddy-viscosity (k–ϵ model) framework, the proposal by Launder et al.[16] is adopted here. To account for the effects of streamline curvature or rotation on length scale, Launder et al. proposed that the coefficient $C_{\epsilon 2}$ in Eq. (17) depends on the Richardson number:

$$C_{\epsilon 2} = 1.92(1 - 0.2Ri) \tag{19}$$

Following Shyy and Ebert,[2] the Richardson number is defined as

$$Ri = -2(k/\epsilon)^2 \Omega_i \omega_i \tag{20}$$

where $\omega_i = \partial U_k/\partial x_j - \partial U_j/\partial x_k$ is the vorticity vector.

It can be clearly observed that turbulence is suppressed if the rotation vector is parallel to the vorticity vector and is enhanced if they are antiparallel.

Numerical Algorithm

The coordinate systems adopted in the present study are either Cartesian or cylindrical, depending on the geometry investigated. The present numerical procedure is based on the finite volume approach and solves discretized versions of all equations over a staggered finite volume arrangement. The principle of mass-flux continuity is imposed indirectly via the solution of pressure-correction equations according to the SIMPLE algorithm.[22] The flow-property values at volume faces contained in the convective fluxes, which arise from the finite volume integration process, are approximated by the quadratic upstream-weighted interpolation scheme QUICK.[23] The solution process consists of a sequential algorithm in which each of the six sets of equations, in linearized form, is solved separately by application of the CGSTAB solver.[24]

At the wall, all of the variables are set to zero, apart from the moving wall velocity, which is set to the same value with the wall or disk's velocity. The treatments at the axis of symmetry simply involve the prescribed zero-gradient conditions for all quantities except the radial velocity, which is zero.

Convergence is judged by monitoring the magnitude of the absolute residual sources of mass and momentum, normalized by the respective inlet fluxes. The solution is taken as having converged when all residuals fall below 0.5%.

Results and Discussion

Turbulent Plane Couette–Poiseuille Flow

Attention is first focused on the effects of the moving wall on the detailed turbulence quantities. Here, the performance of the proposed model is validated against the DNS data for the fully developed plane Couette–Poiseuille flow (see Ref. 25). The schematic of the flow is shown in Fig. 1, where the top wall is at rest and the bottom wall is moving at a constant speed U_w. The Reynolds numbers, based on the channel half-width δ and the bottom wall velocity, are 1800, 2640, and 3000, respectively. Grid densities of sizes 60 and 100 in the direction normal to the wall are used to check the grid independence. Both grids generate similar results; therefore, the 60 grid is adopted. The first grid node near the wall is placed at $y^+ < 1$, to ensure the adequate resolution of the viscous sublayer.

The influence of the moving wall on the flow can be seen by the asymmetric axial velocity U distribution across the channel, as shown in Fig. 2, where the location of the maximum axial velocity is observed to shift toward the moving wall. The velocity distribution near the top wall is similar to that obtained from the fully developed channel flow. However, a markedly different profile is observed at the moving wall region, and the velocity distributions are well predicted by the proposed model, though there is a slight discrepancy in the case with higher wall velocity. Notably, $U_{\tau t}$ and $U_{\tau b}$ are velocities at the top and bottom walls, respectively.

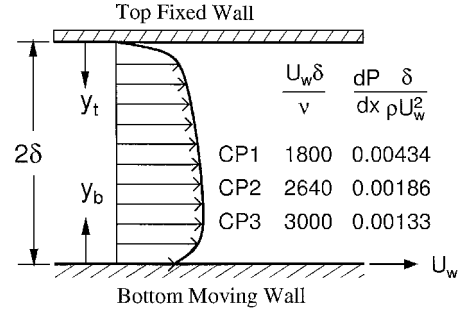

Fig. 1 Geometry of turbulent plane CP flow.

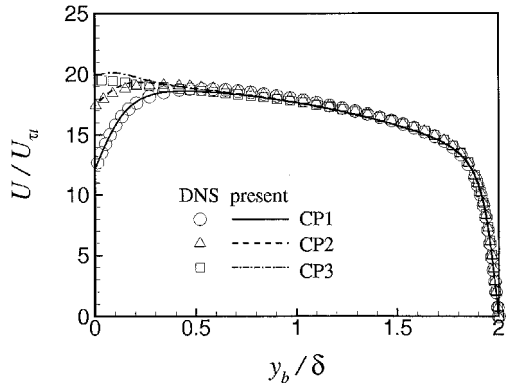

Fig. 2 Mean velocity distributions.

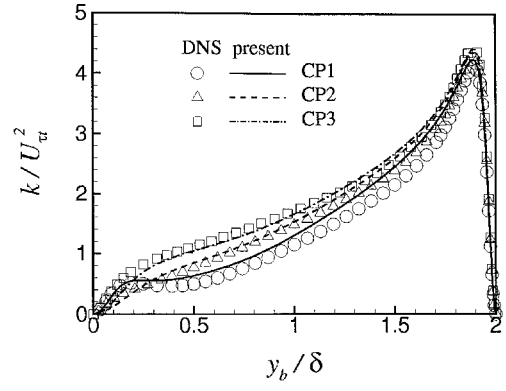

Fig. 3 Turbulence kinetic energy distribution.

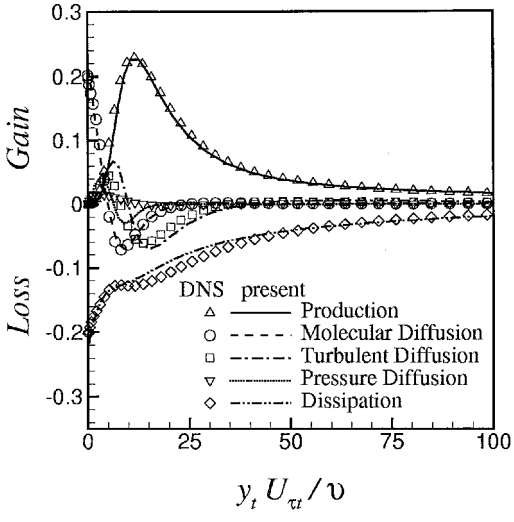

Fig. 4 Turbulence kinetic budget CP2 case, top wall.

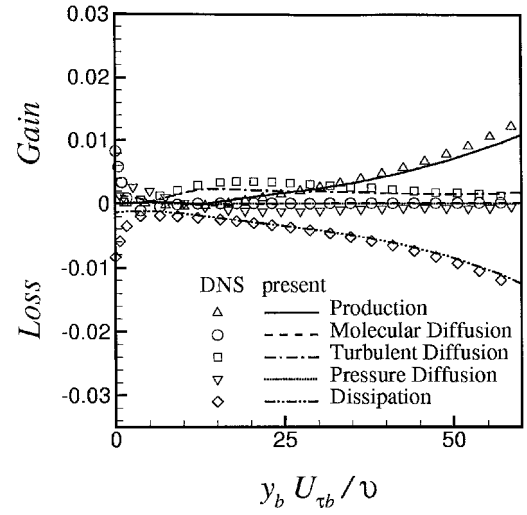

Fig. 5 Turbulence kinetic budget CP2 case, bottom wall.

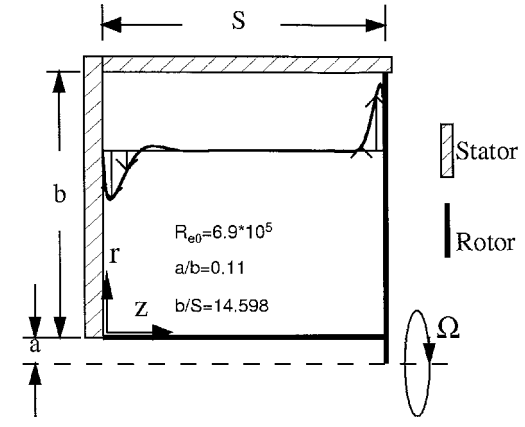

Fig. 6 Geometry of Daily et al.[27] case.

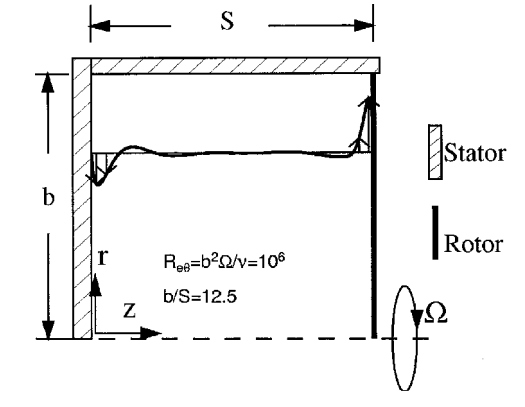

Fig. 7 Geometry of Itoh et al.[26] case.

Because of the reduction of the shear stress at the moving wall, the turbulent kinetic energy adjacent to the bottom wall is severely damped, as can be seen in Fig. 3, compared to the k at the top wall. Finally, the performance of the proposed model can be ascertained by observing the turbulent kinetic energy budgets for the second Couette–Poiseuille (CP2) case, as shown in Figs. 4 and 5.

Rotating Disk Flows

Computations are further applied to rotating disk flows at two different rotational Reynolds numbers to examine the performance of the turbulence models. The geometries of the enclosed disk cavities are shown in Figs. 6 and 7. These consist of a stationary and a rotating disk. Predictions focus on cases in which the rotational Reynolds numbers ($Re_\theta = \Omega b^2/\nu$) are 6.9×10^5 and 1.0×10^6. Notably, the measurements of Itoh et al.[26] indicated that the turbulence on the rotor side is severely damped under that on the stator side.

Numerical meshes, of sizes 100×100, 120×150, and 150×170, are nonuniform in both the x and y directions. The first grid node near the wall is placed at $y^+ < 1$, to ensure the adequate resolution of the viscous sublayer. Preliminary computations of the Itoh et al. case[26] indicate that these three grids predict essentially the same results. The present grid test will be representative because the rotational Reynolds number of the present case exceeds that by the Daily et al.[27] Therefore a grid density of 100×100 is adopted in the computations. The predicted results will be contrasted with measurements by Daily et al.[27] and Itoh et al.[26]

As stated earlier with reference to the rotor–stator cavity flow, the computations of Elena and Schiestel[12,13] showed that the performance of the Reynolds stress transport model is surprisingly similar to that of the eddy-viscosity model on the rotor side, where a reduced

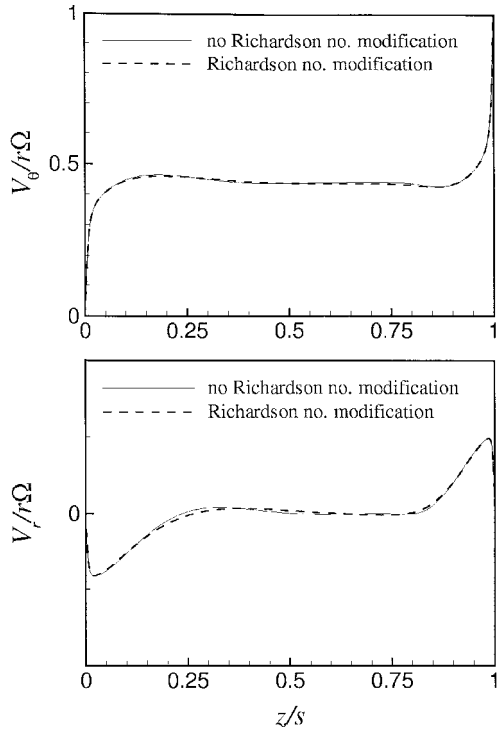

Fig. 8 Tangential and radial velocity at $r/b = 0.8$, effects of modeling of rotation, Itoh et al.[26] case.

level of diffusive transport is predicted. To further pursue the effect of rotation on the flowfield and the turbulence modeling within the eddy-viscosity framework, the rotational Richardson number is used to sensitize the k–ϵ model to rotations.

Figure 8 shows the predicted results of the Itoh et al. case[26] adopting the present model with and without Richardson number modification. The influence of rotation on the turbulence modeling is clearly negligible. Therefore, in subsequent computations, the Richardson number will not be adopted in the model.

Daily et al.[27] *Case:* $Re_\theta = 6.9 \times 10^5$

The case addressed by Daily et al.,[27] for which mean flow measurements are available at several radial locations, is first considered. The response to the representation of turbulence is best exemplified by observing the variation of the radial velocity V_r and tangential velocity V_θ. Outside the thin Ekman layers, the fluid possesses no radial component, as shown in Fig. 9. The tangential velocity, shown in Fig. 10, is seen to remain uniform throughout the core region and varies steeply across the thin near-wall regions.

The LS model shows that the predicted maximum radial velocities on both the rotor and stator sides are similar. This result is not consistent with the measurements, which show that the radial velocity is maximum on the rotor side, due to the lower level of turbulence present in this region. However, the proposed model correctly captures this phenomenon, although there is a discrepancy on the rotor side in the region $r/b > 0.6$, where the model predicts a slightly reduced level of diffusive transport across the Ekman layers.

With reference to the tangential velocity at $r/b = 0.47$, shown in Fig. 10a, the level of the diffusive transport predicted by the proposed

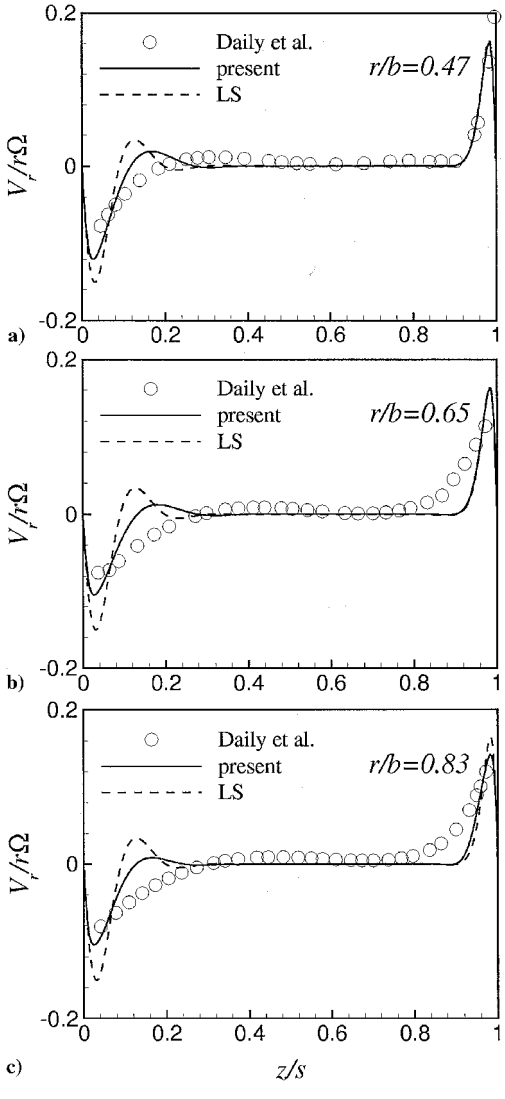

Fig. 9 Radial velocity profiles at various r/b.

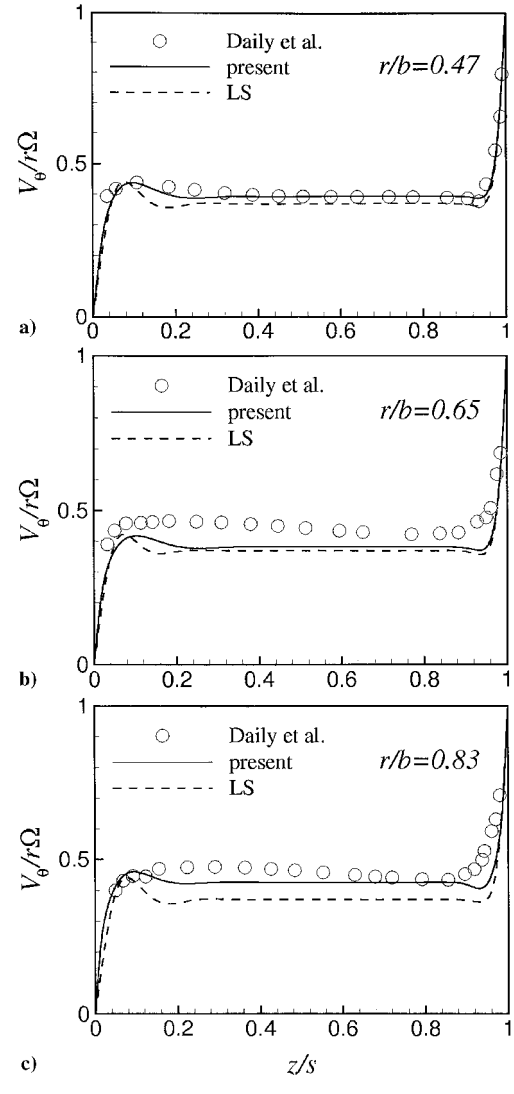

Fig. 10 Tangential velocity profiles at various r/b.

model is further supported by the measurements. The LS model predicts a slightly lower level of entrained tangential component to the cavity interior than was measured. At $r/b = 0.65$, both models predict a lower tangential velocity in the core region than is indicated by the measurements. In the region $r/b = 0.83$, comparisons with measurements indicate that the proposed model shows a correct tangential velocity, whereas the LS model predicts a low tangential velocity.

Itoh et al.[27] *Case:* $Re_\theta = 1.0 \times 10^6$

This case corresponds to a higher rotational number, such that a transition occurs at lower radii than that in the case considered by Daily et al.[27] Figure 11 shows the variations of the radial velocity V_r. Notably, the predictions of the LS model are taken from the computations of Elena and Schiestel.[12]

On the stator side, the present model predicts correctly the development of the Ekman layer, whereas the LS model returns a laminar profile. This LS model behavior was also observed by Morse[4] and Elena and Schiestel.[12] On the rotor side, the measurements indicate a gradual thickening of the Ekman layers from small to large radii because of the transition from laminar to turbulent regimes. The present model does capture this phenomenon, although at small radii, the predicted Ekman layer is too thick, especially at $r/b = 0.4$. The LS model predicts too thin Ekman layer on the rotor side, except

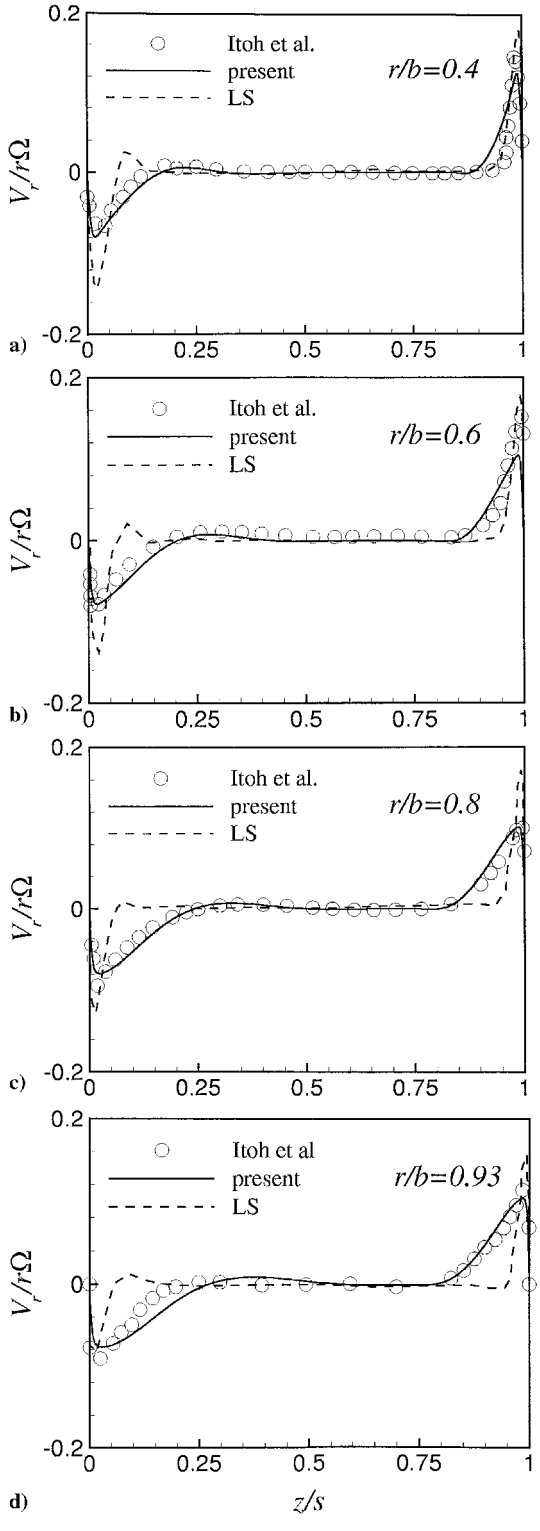

Fig. 11 Radial velocity profiles at various *r/b*.

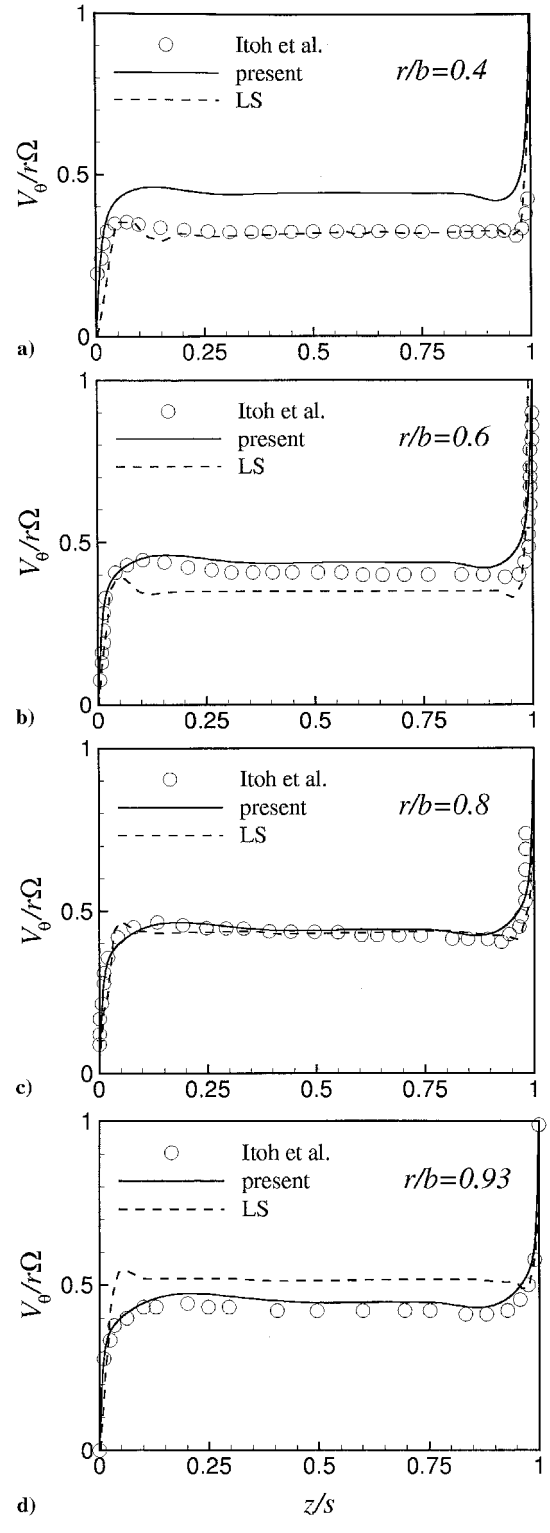

Fig. 12 Tangential velocity profiles at various *r/b*.

at $r/b = 0.4$, where the model correctly predicts the thickness of the Ekman layer.

At $r/b = 0.4$, the flow is laminar due to the relatively low local Reynolds number, and the measurements show that the core fluid rotates at a tangential velocity ($V_\theta/r\Omega$) of about 0.3. Figure 12a reveals that the tangential velocity at $r/b = 0.4$ predicted by the LS model compares favorably with the measured data, whereas the present model shows a higher entrained momentum from the rotor side at this location. This result is consistent with the thickness of the Ekman layer previously predicted by the models, as shown in Fig. 11a, indicating that the present model shows a higher level of diffusive transport and, hence, a turbulent state at this region.

When the Ekman layers are fully turbulent, the core fluid rotates with a uniform tangential velocity of approximately 40% of that of the rotor, as shown in Figs. 12b–12d. The present model accurately predicts the variation of the tangential velocity in these regions, whereas the LS model shows too low and too high tangential velocities at $r/b = 0.6$ and 0.93, respectively.

The Ekman layer was stated earlier to be turbulent on the stator side, and the turbulence is damped on the rotor side. These claims can be verified by observing the polar profiles on the hodograph plane at $r/b = 0.8$ shown in Fig. 13. Figure 13 describes the behavior of the three-dimensional boundary layers on the rotor side and stator side, respectively. The dash–dot lines represent the Batchelor-type laminar flow solutions for infinite rotating disks.[28] Near the rotor, the results of the present model fall very close to the laminar solution and the measurements. In contrast, on the stator side, the polar profile calculated from the present model shows a better agreement with the measurements and differs significantly from the laminar solution. These results suggest that the flow is more turbulent on the stator side than on the rotor side, as predicted correctly by the proposed model.

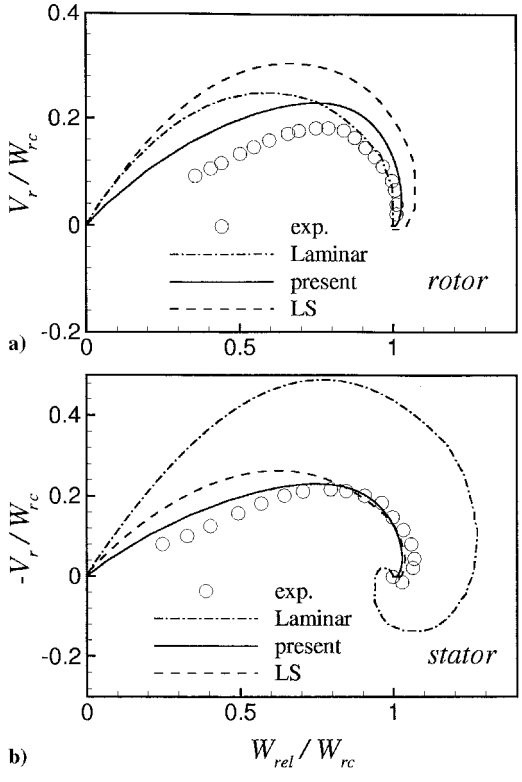

Fig. 13 Polar plots of velocity distribution at r/b = 0.8; tangential velocity relative to the wall, W_{rel}, and value of W_{rel} at midpoint between rotor and stator, W_{rc}.

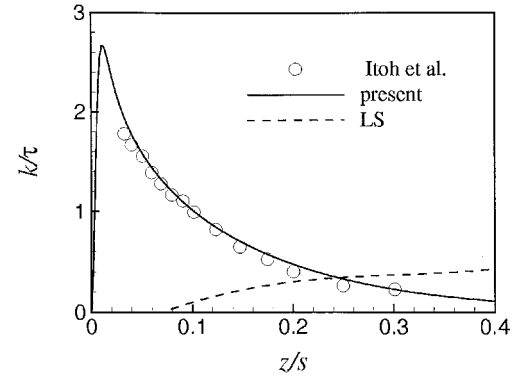

Fig. 14 Kinetic energy profile in the stator boundary layer at r/b = 0.8.

Figure 14 compares the turbulent kinetic energy profiles at $r/b = 0.8$ near the stator wall. The proposed model produces correct turbulent kinetic energy distributions near the stator wall. In strong contrast, the LS model shows a reduced level of turbulence. This result is not surprising, and is reflected by the predicted thin Ekman layer by the LS model, presented in Fig. 11.

Conclusions

An improved low-Reynolds k–$\tilde{\epsilon}$ model is applied to simulate the turbulent flows with nonstationary walls. Major features of the model include the adoption of the Taylor microscale in the damping function and the inclusion of the pressure diffusion terms in both the k and ε equations. The importance of the refined wall modeling is first examined using the DNS data of turbulent plane CP flows. The detailed flow structure is captured accurately by the model, in particular the reduction of the shear stress and, hence, turbulent kinetic energy due to the presence of the moving wall. The proposed model is further applied to enclosed rotating disk flows at two different rotational Reynolds numbers to examine the capability of the model in complex flows. The influence of rotation on the flowfield and the turbulence modeling is investigated by sensitizing the turbulence model coefficient to the rotational Richardson number. The effect is found to be marginal. The internal structure is induced by the diffusive transport of the tangential momentum from the rotor into the interior. Therefore, the predicted thickness of the Ekman layer is found to be critical to the correct predictions. The model correctly reproduced the gradual thickening of the Ekman layers from small to large radii, due to the transition from laminar to turbulent regimes, especially on the rotor side within the disk cavities. The elevated level of turbulence on the stator side compared to that on the rotor side is also predicted correctly by the present model. Conversely, the LS model shows reduced diffusive transport on both sides of the Ekman layers, indicating the importance of refined wall modeling. However, for the case with the elevated rotational Reynolds number, the present model does return excessive diffusive transport at small radii of the disk cavity, where the flow should be transitional.

Acknowledgments

This research work is supported by the National Science Council of Taiwan, Republic of China, under Grant NSC-85-2212-E-007-057, and the computational facilities are provided by the National Centre for High-Performance Computing of Taiwan, Republic of China, which the authors gratefully acknowledge.

References

[1]Owen, J. M., and Rogers, R. H., "Flow and Heat Transfer in Rotating-Disc Systems," *Rotor-Stator Systems*, Vol. 1, Wiley, New York, 1989.

[2]Shyy, W., and Ebert, M. P., "Heat Transfer and Fluid Flow in Rotating Sealed Cavities," *Advances in Heat Transfer*, Vol. 35, April 2001, pp. 173–248.

[3]Chew, J. W., "Prediction of Flow in Rotating Disc Systems Using the $k-\epsilon$ Turbulence Model," American Society of Mechanical Engineers, ASME Paper 84-GT-229, 1984.

[4]Morse, A. P., "Numerical Prediction of Turbulent Flow in Rotating Cavities," *Journal of Turbomachinery*, Vol. 110, No. 2, 1988, pp. 202–212.

[5]Williams, M., Chen, W. C., Bache, G., and Eastland, A., "An Analysis Methodology for Internal Swirling Flow Systems with a Rotating Wall," *Journal of Turbomachinery*, Vol. 113, No. 1, 1991, pp. 83–90.

[6]Morse, A. P., "Assessment of Laminar–Turbulent Transition in Closed Disk Geometries," *Journal of Turbomachinery*, Vol. 113, No. 1, 1991, pp. 131–138.

[7]Iacovides, H., and Theofanopoulos, I. P., "Turbulence Modeling of Axisymmetric Flow Inside Rotating Cavities," *International Journal of Heat and Fluid Flow*, Vol. 12, No. 1, 1991, pp. 2–11.

[8]Hwang, C. B., and Lin, C. A., "Improved Low-Reynolds-Number k–$\tilde{\varepsilon}$ Model Based on Direct Numerical Simulation Data," *AIAA Journal*, Vol. 36, No. 1, 1998, pp. 38–43.

[9]Hwang, C. B., and Lin, C. A., "A Low-Reynolds-Number Two-equation $k_\theta - \tilde{\varepsilon}_\theta$ Model to Predict Thermal Fields," *International Journal of Heat and Mass Transfer*, Vol. 42, No. 17, 1999, pp. 3217–3230.

[10]Hwang, C. B., and Lin, C. A., "Low Reynolds Number k–ε Modeling of Flows with Transpiration," *International Journal of Numerical Methods in Fluids*, Vol. 32, No. 5, 2000, pp. 495–514.

[11]Iacovides, H., and Toumpanakis, P., "Turbulence Modeling of Flow in Axisymmetric Rotor–Stator System," *Proceedings for the 5th International Symposium on Refined Flow Modeling and Turbulence Measurements*, L'Ecole Nationale des Ponts et Chaussées, Paris, 1993, pp. 835–842.

[12]Elena, L., and Schiestel, R., "Turbulence Modeling of Confined Flow in Rotating Disk System," *AIAA Journal*, Vol. 33, No. 5, 1995, pp. 812–821.

[13]Elena, L., and Schiestel, R., "Turbulence Modeling of Rotating Confined Flows," *International Journal of Heat and Fluid Flow*, Vol. 17, No. 3, 1996, pp. 283–289.

[14]Hanjalic, K., and Launder, B. E., "Contribution Towards a Reynolds-stress Closure for Low-Reynolds Number Turbulence," *Journal of Fluid Mechanics*, Vol. 74, 1976, pp. 583–610.

[15]Launder, B. E., and Sharma, B. I., "Application of the Energy Dissipation Model of Turbulence to the Calculation of Flow Near a Spinning Disc," *Letters in Heat and Mass Transfer*, Vol. 1, No. 2, 1974, pp. 131–138.

[16]Launder, B. E., Priddin, C. H., and Sharma, B. I., "The Calculation of Turbulent Boundary Layers on Spinning and Curved Surfaces," *Journal of Fluids Engineering*, Vol. 99, March 1977, pp. 231–239.

[17]Launder, B. E., "Low-Reynolds-Number Turbulence Near Walls," Dept. of Mechanical Engineering, Rept. TFD/86/4, Univ. of Manchester Inst. of Science and Technology, Manchester, England, U.K., Feb. 1984.

[18]Kawamura, H., "A k–ε–v^2 Model with Special Relevance to the Near Wall Turbulence," *Proceeding of the 8th International Symposium on Turbulent Shear Flow*, Technical Univ. of Munich, Munich, 1991, pp. 26.4.1–26.4.6.

[19]Nagano, Y., and Tagawa, M., "An Improved k–ε Model for Boundary Layer Flows," *Journal of Fluids Engineering*, Vol. 112, No. 1, 1990, pp. 33–39.

[20]Patel, V. C., Rodi, W., and Scheuerer, G., "Turbulence Models for Near-Wall and Low-Reynolds Number Flows: A Review," *AIAA Journal*, Vol. 23, No. 9, 1985, pp. 1308–1319.

[21]Savil, A. M., "Some Recent Progress in the Turbulence Modeling of By-Pass Transition," *Proceedings of the International Conference on Near-Wall Turbulent Flows*, Elsevier Science, Amsterdam, 1993, pp. 829–848.

[22]Patankar, S. V., *Numerical Heat Transfer and Fluid Flow*, Hemisphere, New York, 1980, pp. 126–131.

[23]Leonard, B. P., "A Stable and Accurate Convective Modeling Procedure Based on Quadratic Upstream Interpolation," *Computer Methods in Applied Mechanics and Engineering*, Vol. 19, June 1979, pp. 59–98.

[24]Van den Vorst, H. A., and Sonneveld, P., "CGSTAB, a More Smoothly Converging Variant of CGS," Delft Univ. of Technology, TR 90-50, Delft, The Netherlands, 1990.

[25]Kuroda, A., Kasagi, N., and Hirata, M., "Direct Numerical Simulation of Turbulent Plane Couette–Poiseuille Flows: Effect of Mean Shear on the Near Wall Turbulence Structure," *Proceeding of the 9th International Symposium on Turbulent Shear Flow*, Kyoto, Japan, 1993, pp. 8.4.1–8.4.6.

[26]Itoh, M., Yamada, Y., Imao, S., and Gouda, M., "Experiment on Turbulent Flow due to an Enclosed Rotating Disc," *Proceeding of 1st Symposium on Engineering Turbulence Modeling and Experiments*, Elsevier Science, New York, 1990, pp. 659–668.

[27]Daily, J. W., Ernst, W. D., and Asbedian, V. V., "Enclosed Rotating Disks with Superposed Throughflows: Mean Steady and Periodic Unsteady Characteristics of Induced Flow," Hydrodynamic Lab., Rept. 64, Massachusetts Inst. of Technology, Cambridge, MA, 1964.

[28]Batchelor, G. K., *An Introduction to Fluid Dynamics*, Cambridge Univ. Press, Cambridge, England, U.K., 1967, pp. 195–200.

W. J. Devenport
Associate Editor